이학석사 학위논문

Seismic attenuation structure beneath Nazca Plate subduction zone in southern Peru

페루 남부 나즈카 판 섭입대의 지진파 감쇠 구조

2018년 2월

서울대학교 대학원

지구환경과학부

장 효 인

Seismic attenuation structure beneath Nazca Plate subduction zone in southern Peru

지도 교수 김 영 희

이 논문을 이학석사 학위논문으로 제출함
2017년 10월

서울대학교 대학원
지구환경과학부
장 효 인

장효인의 이학석사 학위논문을 인준함
2017년 12월

위 원 장 이 준 기 (인)

부위원장 김 영 희 (인)

위 원 강 태 섭 (인)

Abstract

The subduction geometry of the Nazca plate changes from flat to normal in southern Peru, and cessation of volcanism is observed in the flat slab region. The subduction of Nazca ridge is previously assumed to be responsible for the flat slab development in Peru. We use seismic data from PeruSE, PULSE and CAUGHT which can sample a slab-dip transition zone between the flat to normal-dip slab to estimate seismic attenuation in terms of quality factors, Qp and Qs using P and S phases, respectively. We measure t*, which is integrated attenuation through the seismic raypath between the regional earthquakes and stations. The measured t* are inverted using the least squares method to construct the 3-D attenuation model.

Our Q models from the inversion recover features that can be closely associated with subduction dynamics, slab morphology, and geological features in southern Peru. First, relatively high attenuation is observed in the continental curst continuously from NW to SE in our study domain. Very low Qp and Qs are shown below the volcanic arc and the Eastern Cordilera, which may be related to the presence of melt. Second, high attenuation features in the vicinity of the subducting plate are identified beneath the

volcanic arc, and might be related to the slab dehydration. Also, low attenuation anomaly in the mantle wedge is imaged in the south below a latitude of 18° S, and can be interpreted as the delaminated crustal root. Third, low attenuation in the subducting Nazca plate is imaged throughout the region between the flat and slab-dip transition zone. In particular, shallow-depth high-attenuation anomaly close to the coastal line may be a feature related to hydration of the Nazca ridge.

주요어 : attenuation tomography, Nazca plate subduction zone, Peru
학 번 : 2016-20428

목 차

제 1 장 서 론 1
제 1 절 연구의 배경 1
제 2 절 연구 자료 5

제 2 장 본 론 8
제 1 절 연구 방법 8
제 2 절 해상도 16
제 3 절 연구 결과 18
제 4 절 토의 26

제 3 장 결 론 37

참고문헌 38

표 목차

[표 1] 33

그림 목차

[그림 1] 4
[그림 2] 7
[그림 3] 12
[그림 4] 17
[그림 5] 21
[그림 6] 22
[그림 7] 23
[그림 8] 24
[그림 9] 25
[그림 10] 32
[그림 11] 34
[그림 12] 35
[그림 13] 36

제 1 장 서 론

제 1 절 연구의 배경

The Nazca-South American plate boundary is one of the most typical subduction zones in the world. the Nazca plate is subducting under the South American plate in 8.5cm/yr(Muller et al., 2012) and forms the Andes. Our study area ranges from latitude -20° to -10°, including Southern Peru and little part of Bolivia and Chile(Figure 1).

Of the long convergence boundary across South America, Southern Peru, which is part of our study area, has a somewhat different characters compared to other regions. First, the Nazca plate is subducting to the Altiplano plate, not the South American plate. This plate is a small plate moving slowly to the northeast compared to the South American plate(Bird, 2008). Secondly, our study area is bounded by flat subduction zone in the north and normal subduction zone in the south. Third, the volcanic eruption caused by the Nazca plate subsidence does not extend over the entire subduction zone but has a gap in the middle, which occurs in our study area. The second of these features, the rapid change of the subduction angle in a small area, has attracted many researchers' interest. The Nazca

Ridge located on the boundary of this radical change in dipping angle and also the absence of volcanic arc(Figure 1). The affect of ridge subduction on flat subduction has suggested for many researchers(Gutscher et al., 2000; Martinod et al., 2013), while still in debating(Antonijevic et al., 2015). The distribution of the seismicity are changes in consonance with slab dipping angle changes(Figure 2). the deep earthquakes(>200km) occurs only in normal subduction region. In the ridge subduction region only few earthquakes are occurring.

The average elevation of study area is about 3.5km(Whitman et al., 1996) and the average moho depth is 65km(Ryan et al., 2016). The average depth of the crust is 35km and the average moho depth of more than 60 km do not exist except the Andes and Himalayas(CRUST1.0).

The elevated regions are divided into several geomorphic units(Figure 1). From the little away from the coastline to Altiplano plateau is Western Cordilera, the mountain range of south America including volcanic arc region. And there's Altiplano plateau, one of the highest and largest plateau in the world. Eastern Cordilera located beyond the Altiplano plateau and the subandean fold-thrust belt dividing orogenic region and the others. Crustal shortening are occurring in subandean belt, about rate of 7.5mm/yr of

convergence(Liu et al., 2000; Ramos et al, 2004; Chlieh et al, 2011).

From 2008 to 2013, the PeruSE network has been installed for further investigation of this area. So far, various studies have been conducted on the subduction zone using this data. We use the same data to measure the degree of seismic attenuation to see the properties and structure of subduction zones. We also use several other seismic networks to explore a wide area where the angle of subduction changes, and we will look at how the structure changes using 3-dimensional tomography.

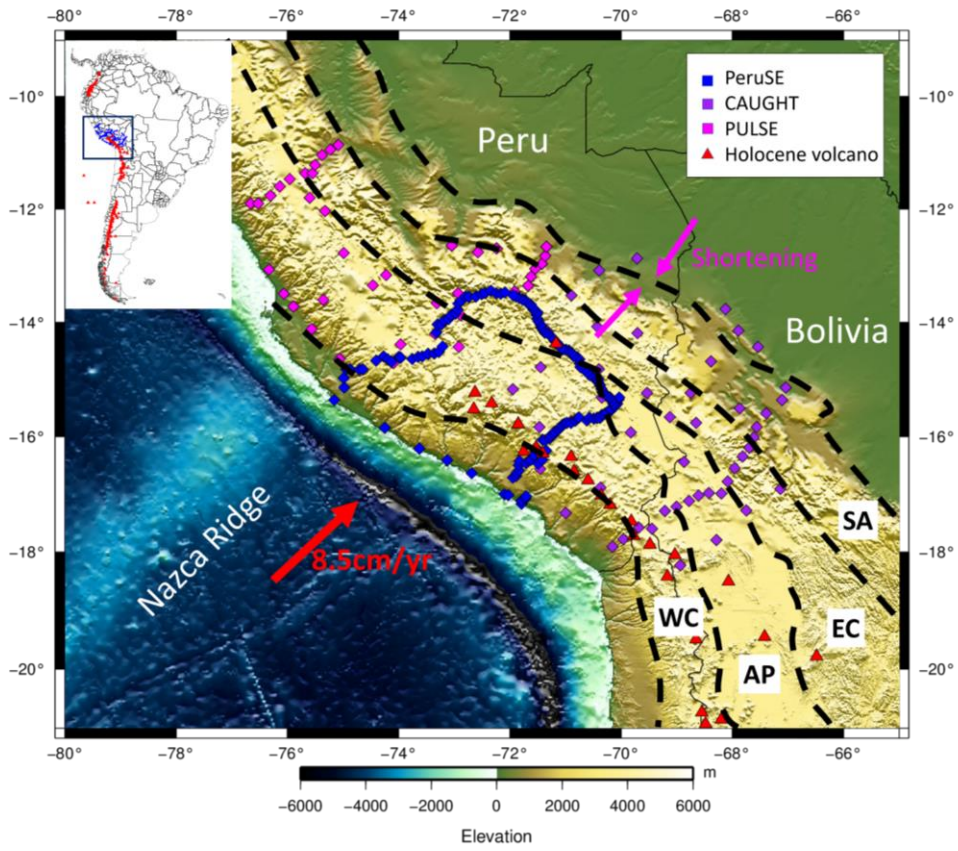

Figure 1. A map showing stations and geomorphic units. Geomorphic divisions, staions are displayed. Red triangle line is convergence boundary(Bird, 2008). SA denotes subdandean fold−thrust belt, EC eatern Cordilear, AP Altiplano plateau and WC western Cordilera.

제 2 절 연구 자료

We used 3 broadband networks (PeruSE(TO), CAUGHT(ZG) and PULSE(ZD)) to obtain earthquake waveform(Figure 1). Peru Subduction Experiment(PeruSE) operated from July 2008 to April 2013 above the southern Peru subduction zone. Peru Lithosphere and Slab Experiment (PULSE) and Central Andes Uplift and Geodynamics of High Topography (CAUGHT) were deployed in 2010−2013 across southern Peru to Bolivia.

The earthquakes were referenced NEIC and ISC catalogues. The magnitude of events are restricted to 4.0−6.5 and the depth are ranged from 20km to 300km(Figure 2). In comparison with the location of the reference catalogues and the earthquake relocation results from Lim et al (in prep), quite differences were observed in a horizontal scale by 0.4 and a vertical scale by 50km. In this study, we simply relocated events after manual picking to overcome these differences. We used Hypoellipse(Lahr, 1999; modified by T. Kang) based on the velocity model of Phillips et al.(2012) and performed 1000 bootstrapping to find out and to minimize the effect of the wrong picking. We excluded all earthquakes that could not be relocated due to insufficient number of pickings or calibrated to outside the given range. Finally, we get 384 earthquakes having

lower differences from the earthquake catalogue of Lim, about 20km(Figure 2).

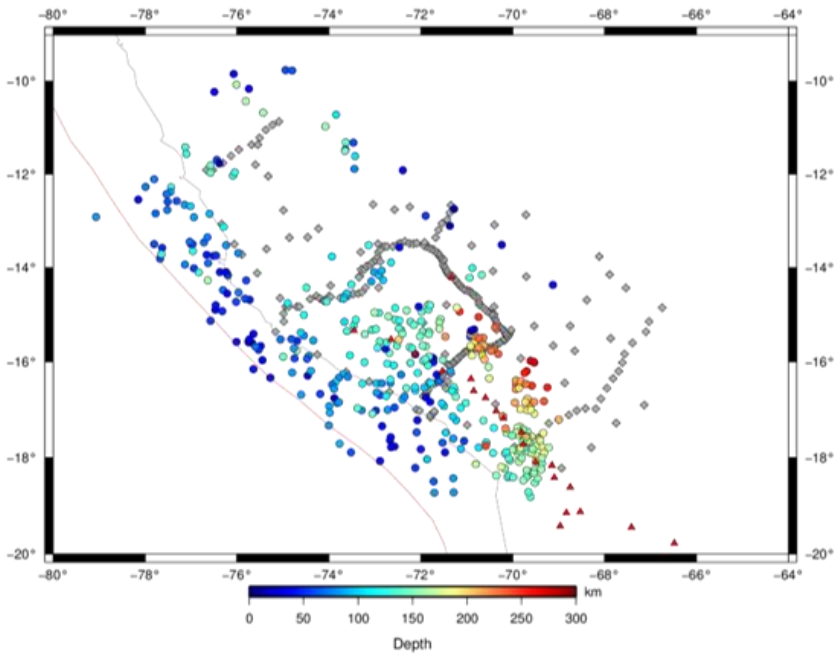

Figure 2. Map of relocated events. We used 383 earthquakes occurred from 2008 to 2013 whose magnitude ranges 4.0−6.5 and depth shallower than 300km. 19487 S wave 27796 P wave are used and every arrivals are manually picked.

제 2 장 본 론

제 1 절 연구 방법

제 1 항 Definition of seismic attenuation

Seismic waves lose their energy during their passage though underground materials due to scattering and intrinsic attenuation. The intrinsic attenuation occurs in the presence of volatile, fluid contents, partial melting or high temperature, grain size of minerals and viscosity. Seismic attenuation is quantified as Q, which represents the ratio of energy lost during one cycle to total wave energy.

$$Q^{-1} = \frac{\Delta E}{2\pi E}$$

(Eq. 1)

1/Q is proportional to the grain size, enclosed melt/H20 content ratio, and temperature. (*Faul et al. 2004; Aizawa et al., 2008*). Q is also considered as a damping factor in damped harmonic oscillator model, which can be expressed as Eq.2 (*Stein and Wysession, 2009)*. If the material has low Q, it means high attenuation, and vice versa.

$$x(t) = Ae^{-\omega_0 t/2Q}\sin(\omega t)$$

(Eq. 2)

where A represents an initial amplitude, w_0 a natural frequency, t time, w frequency, and x amplitude.

Since high attenuation is deeply related to melting process provide meaningful constraints on physical parameters of magma chamber and/or mantle wedge beneath the volcanic arc. We develop numerical framework to quantify seismic attenuation (in terms of a quality factor, Q).

제 2 항 Measuring t* value

Seismic attenuation is quantified as a quality factor Q, which represents the ratio of energy lost during one cycle to total wave energy (Eq. 1). The Q is power law frequency dependent value that commonly expressed as

$$Q = Q_0 f^{-\alpha}$$

(Eq. 3)

where α constant and $Q0$ quality factor when frequency is 1 Hz. The α is fixed as 0.27 as other subduction zone attenuation

researches(Stachnik et al., 2004; Rychert et al., 2008). The Q averaged along the raypath is denoted as t^*.

$$t^* = \int_{raypath} \frac{dr}{Q(r)\,V(r)}$$

(Eq. 4)

where V denotes velocity.

The frequency range is 0.5−30 and we used 2.56seconds after each P and S phase arrivals. Then we applied the multi−tapering method (*Prieto et al., 2009*) to change the time domain to frequency domain. Every arrival times are manually picked and we used not very clear arrivals that could not be used to locate the events to obtain more attenuated signals, and the criteria for signal to noise ratio is 1.5. The number of P and S signals used in inversion is 27756 and 19487, respectively.

A theoretical velocity spectrum A in ith station for a jth event (*Anderson and Hough, 1984*) is

$$A_{ij}(f_n) = CS_j(f_n)B_{ij}(f_n)I_i(f_n)$$

(Eq. 5)

where C constant, S source spectrum, B attenuation along the raypath and I instrument response. We assumed ω^{-2} type source model (*Brune, 1970*) for the source S.

$$S_j(f_n) = \frac{f_n M_{0j}}{1+(f_n/f_{cj})^2}$$

(Eq. 6)

where *f* frequency, *M0* seismic moment and *fc* corner frequency. *B* is expressed as

$$B_{ij}(f_n) = \exp(-\pi f_n t^*_{ij}).$$

(Eq. 7)

We neglected *I(f)* term considering selected frequency range (*Chen and Clayton, 2008*). Adding up Eq. 5−7, we now have

$$A_{ij}(f_j) = \frac{C' f_n}{1+(f_n/f_{cj})^2} exp(-\pi f_n t^*_{ij})$$

(Eq. 8)

where *C'* constant.

We applied more than 10 iterations to determine stable *t** as suggested by Eberhart−Phillips and Chadwick (*Eberhart−Phillips and Chadwick, 2002*) (Figure 3). We discarded unreasonable *t** values that are not positive values or too large.

We determined one corner frequency for one event by grid searching. We stacked all waveforms for one event considering SNR and obtained corner frequency of each event using fixed *t**. Each corner frequency of P and S phase are measured separately.

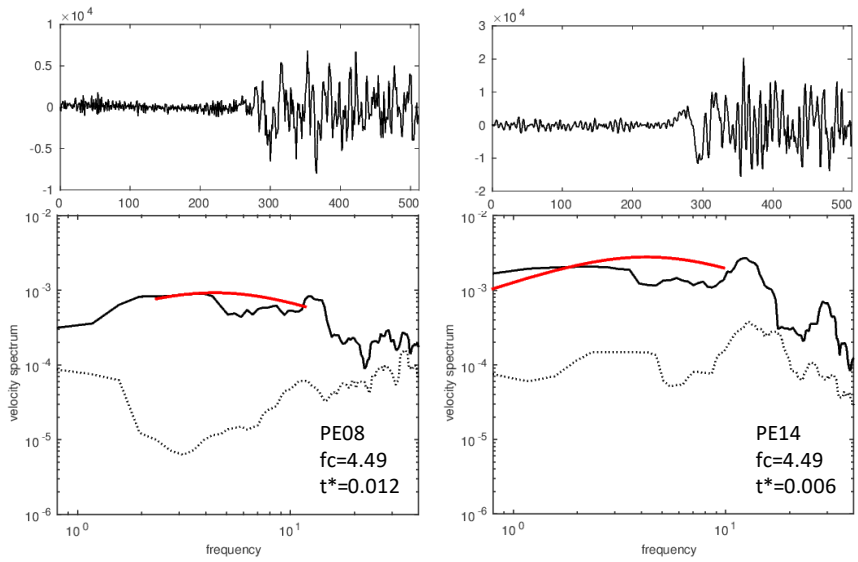

Figure 3. Example showing the fitting of velocity amplitude spectrum of one local earthquake. Signal and noise velocity spectra are shown as solid and dotted black lines, respectively. Fitted spectrum line is shown as a thicker solid line.

제 3 항 Tomographic Inversion

We inverted obtained $t*$ measurements for 3-D quality factor structure. We discretized the Eq. 4, assuming that each block has constant $1/Q$ and V. The raypath of each event and station was calculated using taup module of ObsPy. The velocity of each grid is based on Philips model. We tried out previous researchers' Peruvian velocity structure models. We used Ma and Clayton, Philips and IASP91,and used the model that best matched the manual picking results for each phase arrival time. The Q was estimated by damped least square method, which minimized a combination of data misfit and average model norm using obtained $t*$ (Eq.9; *Tarantola, 2005; Menke 2012.*).

$$m = [G^T W_e G + \eta^2 W_m]^{-1} [G^T W_e d + \eta^2 W_m m_{model}]$$

(Eq. 9)

where d denotes observed dataset, m the property of each grid, G the relationship between m and d, m_{model} the starting model that has uniform value 200, We and Wm the weighting factor, and η damping factor. The weighting factors contained quality of the fitting and SNR.

When there are more solutions to the inverse problem, the problem is considered as ill-conditioned, and in such case, the

regularization should be incorporated to prevent overfitting. For the parameter regularization, we used L-curve test to determine the damping factor, η. The L-curve test is a log-log plot of the norm of the regularized solution versus corresponding residual norm. It is a trade-off curve between the two factors often shapes like 'L' and the corner of the 'L' is selected to meet the criterion. For strictly locating the corner of the L-curve, we used a point with the maximum curvature in the curve (*Hansen et al., 1999*).

Quality of the inversion method could be tested by the checkerboard test. In this checkerboard test, we altered the model by a regular pattern of 50 and 500 like a checkerboard (Figure 13). This perturbed model was then used to calculate t^* at all the data points. These t^* became the observed data of the resolution test (Figure 4). The quality of the inversion was proportional to ray path coverage, and thus locations of regional earthquakes were one of important factors which controlled the resolution at deeper depth.

The stations and the events are unequally distributed in wide range. We did grid search to determine inversion grid range to minimize grid size and computation time. The grid size is wider in the edge(Horizontally, 0.45 degrees in boundary area and 0.3 degrees in other area. Vertically, 20km deeper than 240km and 15km in shallower depth) considering distribution of events(Figure

2). We also considered elevation of stations which locate over the Altiplano plateau.

제 2 절 해상도

The checkerboard test results are displayed along the depth in Figure 4. One block of the input data ranged 0.6° horizontally and 30km vertically. The resolution of P wave is better than S wave over all depth. The result resolved down to 250km but the resolution greatly depend on location of events and stations. The resolution of the top of the model(depth <30km) is strongly restrained to regions neighboring stations. Intermediate depth(30-100km) resolution is comparative good except nearby subducting the Nazca ridge cause of lack of earthquakes. In the deeper depth (100-250km), the resolution is controlled by location of deep events, mostly occurred in the eastern side of the grid. The density of the raypath over the depth 150km is simply imaged as figure #. Overall, recovered values are slightly overestimated, but in the reliable error range.

We set the range of reliable resolution to be less than 15% difference between the reconstructed value and the inputted value.

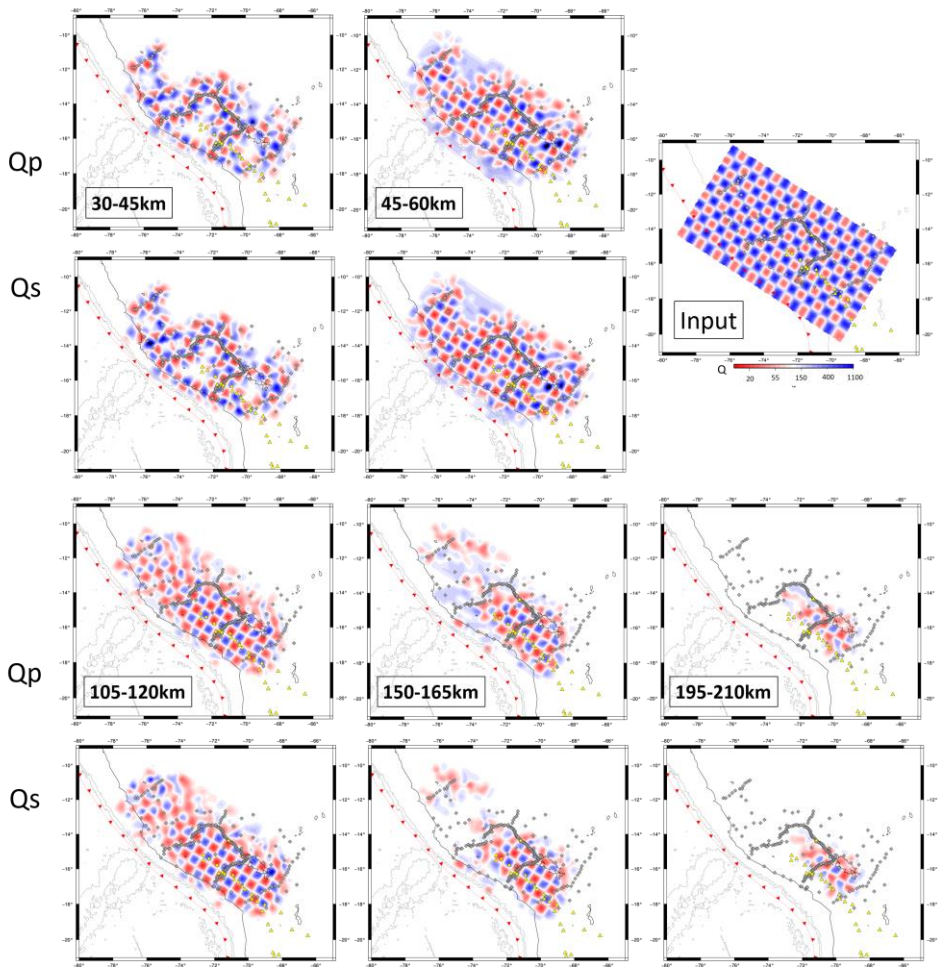

Figure 4. Checkerboard test of Qp and Qs inversion.

제 3 절 연구 결과

We obtained the horizontal and vertical sections at the various positions of the computed 3 dimension attenuation tomography, and the results are shown throughout the figure 7−9. In the case of the horizontal section, the contour of the slab (referenced slab1.0 from Hayes et al., 2012) corresponding to each depth is shown as 5 km depth intervals and in the vertical section, the slab in displayed as black line. The crust−mantle boundary(referenced CRUST1.0 model from Laske et al., 2013) is displayed as black dotted line and the elevation of the crust was expressed as well. We used two different colorbars with 60km depth as the boundary.

In both sections, the limit of resolution is represented by a purple line.

We can see that Qp and Qs values above the moho boundary is higher than the lower ones. Considerably low Qp and Qs values are also observed in some areas, which correspond to areas just below the volcanic arc and Eastern Cordilera. We will discuss this in the discussion. These high−value boundaries coincide well with the crust−mantle boundaries. This coincidence occurs in all regions regardless of slab angle. However, low attenuation values beyond

the moho boundary below the eastern Cordilea or under the volcanic arc are also shows and will be discussed in the discussion.

The comparison with the slab is easy to see from the vertical section. Unlike moho, the relationship between slab and attenuation varies depending on the location. In figure 5, the study area was divided into three areas according to the slab subduction angle.

From the horizontal figures we could identify high Qp and Qs value nearby the slab contour down to 100km regardless of slab subducting angle. Below the 100km layer, the Q value distributed complicated especially in Qp structure.

In the flat subduction area, high Qp and Qs value appears relatively clearly below the slab boundary. The highly attenuated anomaly under the slab line in depth 30−70km is also shown, with high seismicity, and we will talk about it and other anomalous features in discussion. In slab angle transition zone, structure is more complex than the flat subduction zone, seems like low attenuated structures are going upward compared to the slab line. From the more detailed research on the flat slab region than the slab1.0 model, the flat slab rises (*Dougherty and Clayton, 2014*) 2−30km where about 400km away from the trench. It is also shown *in Ma and Clayton,(2014)* and *Lim et al., 2016 (In prep).*

In the normal subduction area, we could find lowly attenuated

structure under the slab line in shallower(<100km) depth. However in deeper region, it is hard to identifying slab only using the Q structure, not with seismicity. We will discuss these complex structure in the discussion.

The Q values of slab is diverse according to the location. in the northern area, the Qp and Qs are both very high (Qp : 500−1000, Qs : 500−700). in the flat subduction zone near the Nazca ridge, Q value is little lower than the northern area(Qp : 200−500, Qs : 200−300). In the normal subduction zone, the Q value is higher than the flat slab(Qp : 300−650, Qs : 300−550).

According to the subduction zone models, the mantle wedge is existing between the crust and the slab. In the flat subduction zone, the interval between slab and the crust region is too narrow to argue about the structure.

The mantle wedge could be found in normal subduction zone, values of Qp are 60−120 and the Qs are 90−120, which is similar to the neighboring subduction zone researches(Qp : 80−150, Andes, *Schurr et al., 2003*; Qs : 76−78, Nicaragua, Qs : 84−88, Costa Rica, *Rychert et al., 2008*; Qs : 90−110, Andes, *Myers et al., 1998*;).

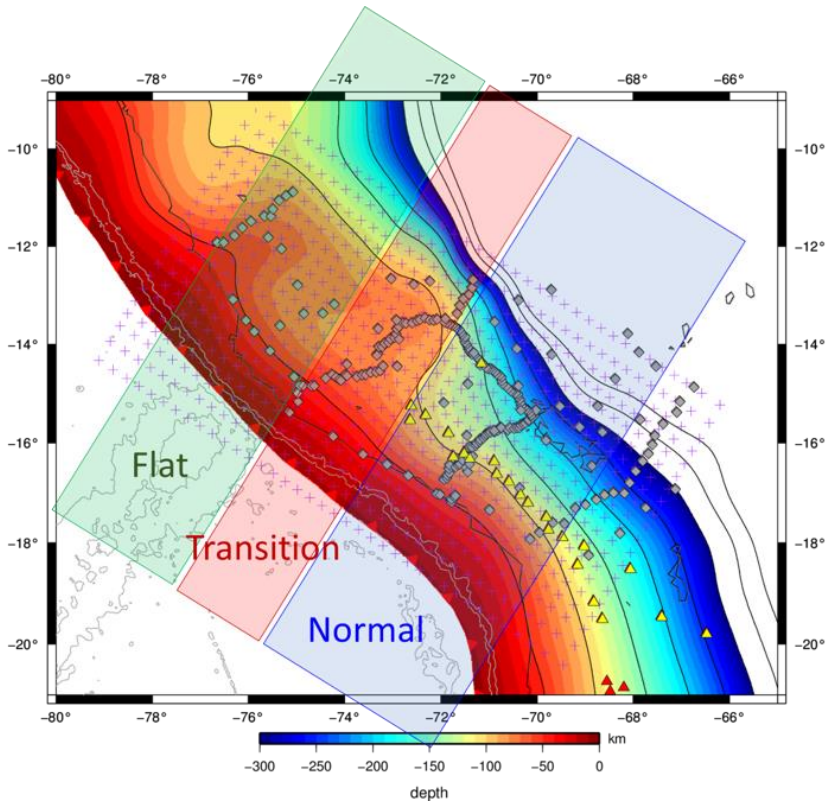

Figure 5. Slap-depth contour (Hayes et al., 2012). Purple cross indicates grid used in inversion.

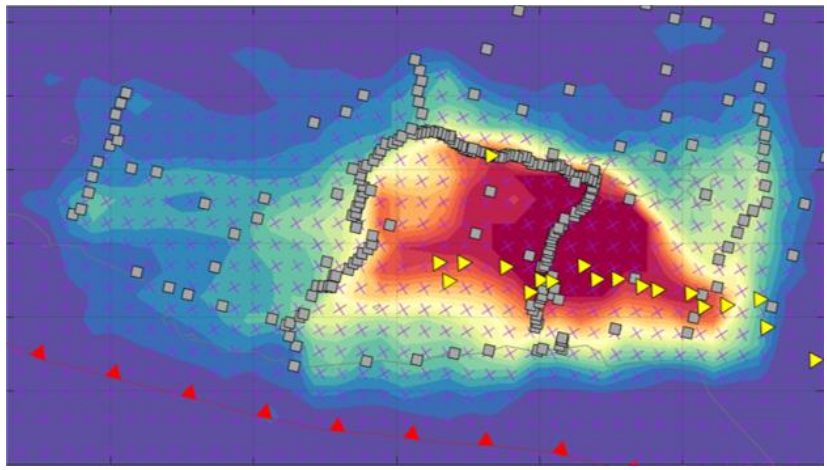

Figure 6. Raypath density in depth shallower than 150km. Red color indicates high density, blue color indicates low density.

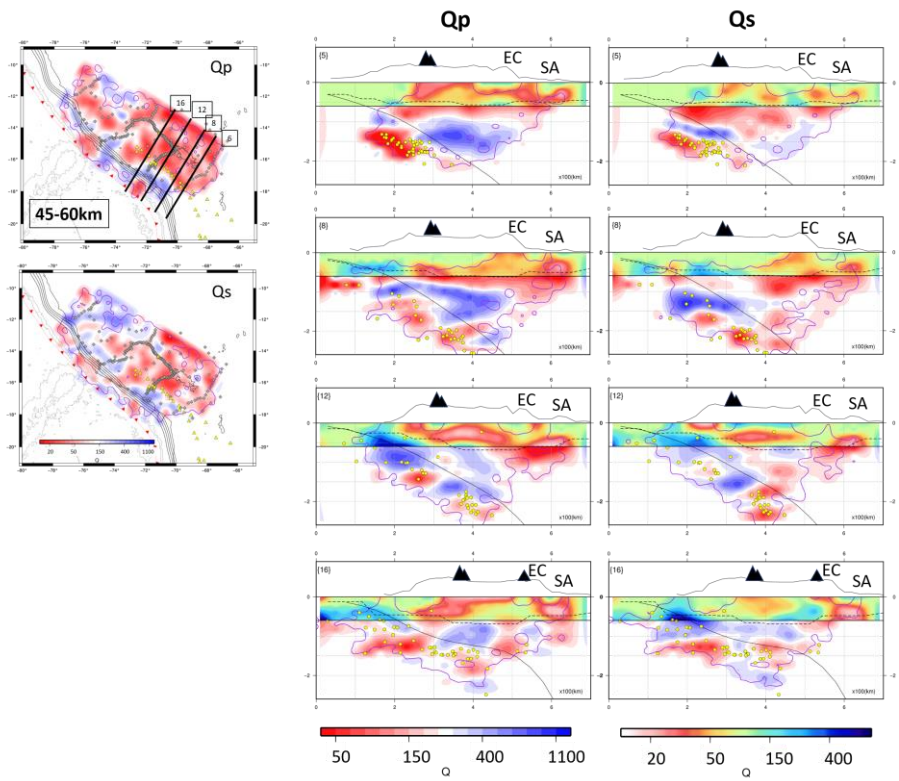

Figure 7. Horizontal and vertical profiles of Qp and Qs in the normal subduction area. Yellow circles denotes nearby events, thick black line slab, dotted black line moho and purple line good resolution boundary. Double black triangle is volcanic arc and single black triangle is the Quimsachata volcano.

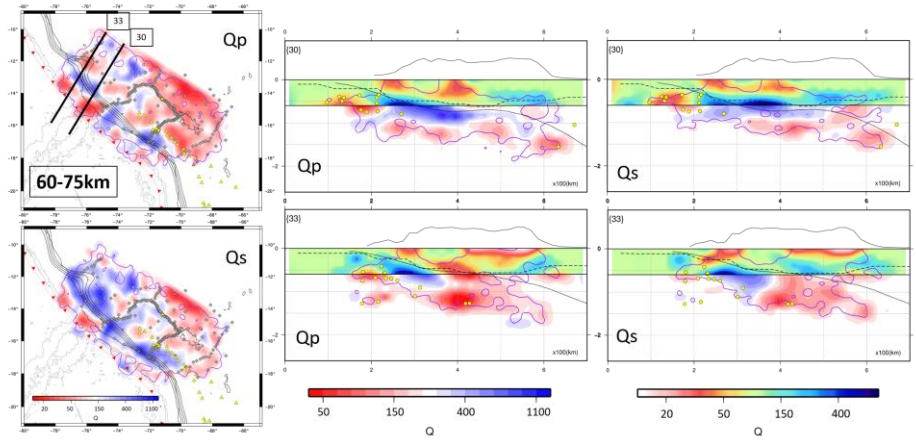

Figure 8. Horizontal and vertical profiles of Qp and Qs in the flat subduction area.

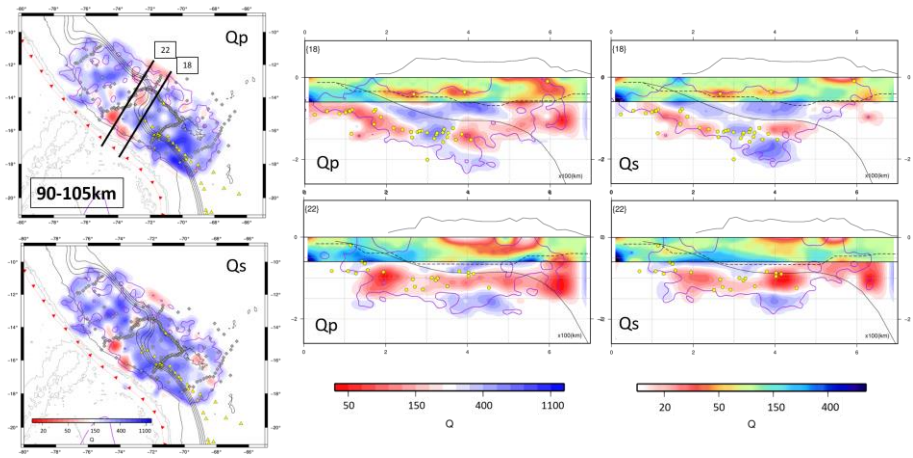

Figure 9. Horizontal and vertical profiles of Qp and Qs in the subducting angle transition zone.

제 4 절 토의

We observed considerably highly attenuated anomaly(Qp: 20−30) below the volcanic arc. The arc volcanoes are erupting vigorously today (Figure 10, Table 1). Other volcanoes whose name is not on the list erupted in Holocene. In the horizontal profiles of depth range 15−60km, the high attenuation structure are distributed directly beneath the volcanic arc. The highly attenuated anomaly located near the Andahua and Sabancaya(Figure 7,10), where the valley with three composite volcanoes(Andahua, Orcopampa and Huambo). These volcanoes are comprised of mafic rocks, and the origin of the melt thought to be located in the lower crust *(Delacour et al., 2007)*, which is correlate with our high attenuation location. The anomaly extended beyond the moho boundary and connected to the slab structure, welly displayed in the Qp result, and more weekly seen in the Qs result, in figure 7. The highly attenuated area in the slab is about 100km, 300km away from the trench. The similar structure are shown in nearby region studies(*Myers et al.,1998; Harberland and Rietbrock, 2001; Schurr et al., 2003; Kay and Coira, 2009; Bianchi et al., 2013; Schurr et al., 2006; Heit et al., 2008a;*). Many studies explained it as dehydration and decompression melting process related to the volcanic arc eruptions.

The ground for dehydration was the high Q, linked to the volcanoes, high seismicity(*Dobson et al., 2002*) and low velocity.

Not only beneath the Andahua and Sabankaya, the vertical profiles under the volcanic arc shows similar pattern that the crust and slab linked by low attenuation. The vertical profile 5 shows good coincidence with the dehydration features. There's two locations that slab interacting, 1) 100km depth 300km away from the trench and 2) 200km depth 400km away from the trench(Figure 13). Harberland and Rietbrock(2001) also found similar Qp structure in Southern area and suggested that the origin of two structure is dehydration(Figure 10 in Haberland and Rietbrock, 2001). However in our study, interestingly, in some vertical profiles Qp and Qs shows different pattern in the same location. These phenomena usually occurred in the pattern 1. In most cases, pattern 1 is clear by Qp, little or not shown in Qs, and the pattern 2 are welly shown in Qs, little shown in Qp. We tried to reconstruct the slab with the slab structure input to ensure the reliability of this shape, and as a result we were able to obtain a fairly well reconstructed slab(Figure 12). From theoretical definition of Q,

$$1/Q_p = (1-L)Q_\kappa + L/Q_s$$

(Eq 10)

where

$$L = (4/3)(V_s / V_p^2)$$.

(Eq 11)

Qk bulk attenuation(Anderson, 1989). If the bulk attenuation is negliable, Qp/Qs in the mantle would be 2.2−2.6(*Pozgay et al., 2009*). If the ratio would be smaller that the value, the bulk attenuation is not negliable. In the many studies on the subduction zone, the Qp/Qs ration are shown lower value than that, 1.75 in Tonga Fiji(Roth et al., 1999), 1.2 in mariana(*Pozgay et al., 2009*), 2.15 in Philippine see(*Shito and Shibutan, 2003*), 1.2−1.4 in Alaska(*Stachnik et al, 2002*) and others. In our study, the best fitting Qp/Qs ratio is about 1.5(Figure 17), which implies effect of bulk attenuation. But our discordant anomaly shows very low very low Qp/Qs ratio, even goes down to 0.33. Further study would needed to explain the discord.

We can observe highly attenuated area beneath the Eastern Cordilera and the Altiplano plateau. Low velocity zone were reported by Dorbath et al., 1993, in the same depth and the location (~70km), thought as mantle upwelling. Low velocity zone under the eastern Cordilera are found in many studies *(Beck and Zandt, 2002, Elger et al., 2005; Heit et al., 2007; Kay and Coira, 2009; Asch et al., 2006; Schurr et al., 2006; Myers et al., 1998)* in the Chile and Bolivia where the south of our study area. The low velocity zone in

the mid-crust area are shown in receiver function and velocity tomography. The Eastern Cordilera thought to be made in mid-Oligocene, 30-24Ma. The large magmatism, called as the Tacaza arc was generated by the arc back-migration that induced mantle upwelling and decompression(*Mamani et al., 2010*). After the magmatic era, newly made magmatic rocks are found in the Eastern Cordilera and the Altiplano plateau, some of them are recently made(<2Ma)(*Carlier et al., 2005*). Carlier said the source of the rocks are complex and seems to have several origins and one(K-AK melt) of them is the melt in shallow depth(<100km) and suggested older lithospheric weakens zones like Cusco Vilcanota fault system make leakage of melt. The Quimsachata volcanic rocks are belonged to these case(*Carlier et al., 2005*). From the vertical profiles the low Qp and Qs structure is related to the mid-crust low velocity zone which thought as melt in many studies, located in depth 30-70km.

In the figure 7, we can observe high Qp and Qs anomaly located in depth below 100km, up to the slab line. This structure only seen in normal subduction zone. These structure is not the slab considering depth, shape and seismicity. The similar structure are shown in *Scire et al., 2015*, anomaly C and D in Figure 13 and Ward et al, 2016. Also the low attenuation or high velocity structure in the

mantle wedge are shown in southern region(chile and Bolivia) in other studies(*Schurr et al.,2006; Beck and Zandt, 2002; Bianchi et al, 2013*;). They suggested it as removal of lithosphere. Kay and Kay suggested delamination and related magmatism model in Andes. They said the crustal thickening result from the shortening make crustal density high, may higher than below mantle lithosphere, and result in delamination. The delaminated crustal root drives rapid uplift of under a region which makes great effects on mantle-derived magmatism. It appears in Southern Puna Plateau, where south of our study area. We made schematic figure illustrating dehydration and delamination structure in the normal subduction zone(Figure 13).

Unlike the southern part of the study area is very similar to the central Andes study results, northern part, where the flat subduction zone, features different anomalies. In the figure 8, we can observe high attenuation zone(Qp : 50-150, Qs : 50-150) located in depth range 20-70km, very close to the trench, under the slab line with high seismicity. This structure are also shown in velocity studies(*Ward et al., 2016; Antonijevic et al., 2015*;). From our previous discussion on the slab dehydration(high attenuation, low velocity, high seismicity), the anomaly is also the dehydration structure even though none volcanic region. The anomaly occurs

throughout where ridge subducting. Cause of our limitation on resolution, it is unclear that anomaly only occurred in ridge region. From Dougherty and Clayton, thin ultra-slow velocity layer presented in that area(45-100km, thin as 3km). They explained it as effect of high hydration by the Nazca ridge, resulted in localized talc-rich dehydration. The anomaly in our study also could explained as hydration from the ridge.

In the vertical profile 33 in figure 8, we could see highly attenuated region on the slab line, where starting to bend. Unfortunately, the resolution beneath break location is too poor to identify if these anomaly is teared slab or not.

In the figure 9, the slab angle transition zone, the vertical profile structure is complex of several high and low attenuation regions. We can observe highly attenuated area below slab or within the oceanic mantle(Qp : 50-150, Qs : 50-150). It would be the oceanic mantle but the considerably low Qp and Qs for mantle would suggest that anomaly would indicates mantle flow due to dipping angle change, still need more research to make sure.

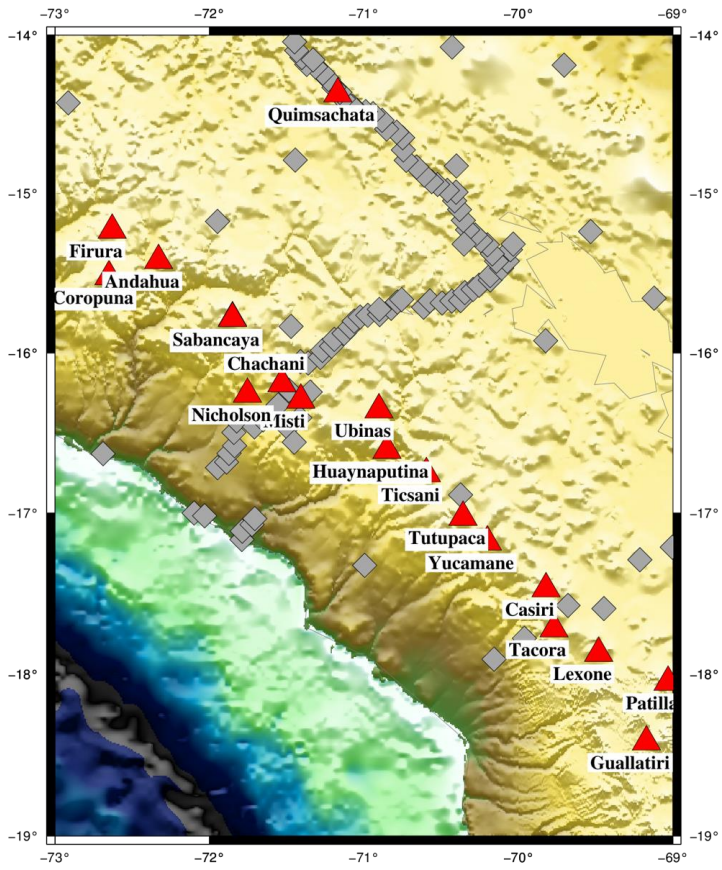

Figure 10. The name of the Volcanoes.

Volcano	Last eruption
Andahua	1490
Misti	1985
Sabacaya	2017
Quimsachata	-4450
Ubinas	2017
Huaynaputina	1600
Tiscsani	1800
Yucamane	-1320
Guallatiri	1960

Table 1. Last Eruption year of volcanoes which have historical eruption.

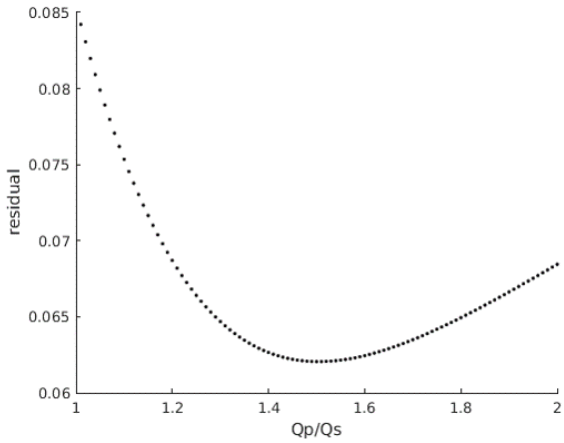

Figure 11. Best fitting Qp/Qs ratio of our study.

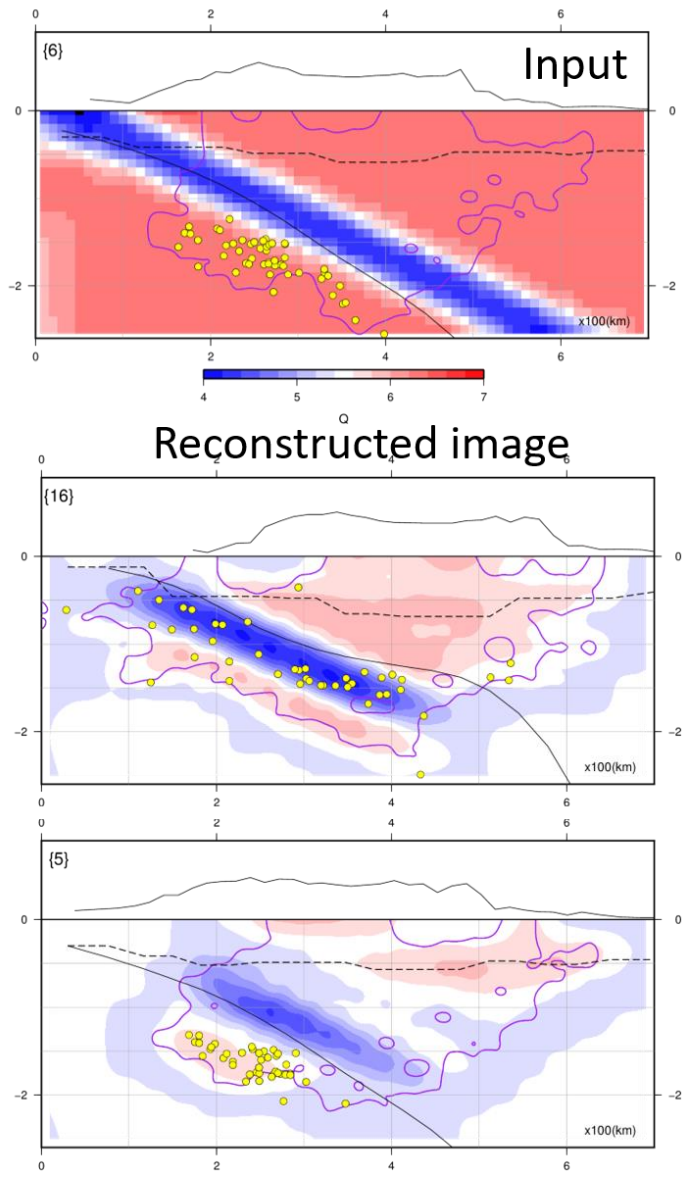

Figure 12. Recovering test for the slab in the normal subduction zone

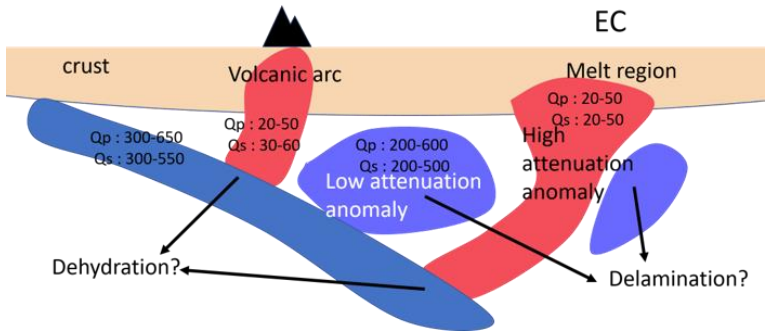

Figure 13. Schematic image for the structure beneath crust in the normal subduction zone.

제 3 장 결 론

We have investigated the complexity of the structure below the Southern Peruvian subduction zone through seismic attenuation studies. We related geochemical properties such as surface volcanic arc and volcanic eruption histories with attenuation structure in the crust and slabs. In the normal subduction zone, we could see similar structure with the central subduction zone, such as dehydration and delamination. In the flat subduction zone, there are unique hydration anomaly thought to be influenced by the Nazca ridge. However, in the area where slab subducting angle changes, sufficient discussion could not be done.

참고 문헌

Abers, G. A. (2000). Hydrated subducted crust at 100–250 km depth. Earth and Planetary Science Letters, 176(3), 323–330.

Aizawa, Y., A. Barnhoorn, U. H. Faul, J. D. FitzGerald, I. Jackson, and I. Kovacs (2008), Seismic properties of Antia Bay Dunite: An exploratory study of the influence of water, J. Petrol., 49(4), 841–855.

Anderson, J. G., and Hough, S. E., 1984, A model for the shape of the Fourier amplitude spectrum of acceleration at high frequencies. Bulletin of the Seismological Society of America, 74(5), 1969–1993.

Antonijevic, S. K., Wagner, L. S., Kumar, A., Beck, S. L., Long, M. D., Zandt, G., ... & Condori, C. (2015). The role of ridges in the formation and longevity of flat slabs. Nature, 524(7564), 212–215.

Asch, G., Schurr, B., Bohm, M., Yuan, X., Haberland, C., Heit, B., ... & Pardo, M. (2006). Seismological studies of the Central and Southern Andes. The Andes, 443–457.

Beck, S. L., & Zandt, G. (2002). The nature of orogenic crust in the central Andes. Journal of Geophysical Research: Solid Earth, 107(B10).

Bianchi, M., Heit, B., Jakovlev, A., Yuan, X., Kay, S. M., Sandvol, E., ... & Comte, D. (2013). Teleseismic tomography of the southern Puna plateau in Argentina and adjacent regions. Tectonophysics, 586, 65–83.

Brune, J. N., 1970, Tectonic stress and the spectra of seismic shear waves from earthquakes. Journal of geophysical research, 75(26), 4997–5009.

Carlier, G., Lorand, J. P., Liégeois, J. P., Fornari, M., Soler, P.,

Carlotto, V., & Cardenas, J. (2005). Potassic–ultrapotassic mafic rocks delineate two lithospheric mantle blocks beneath the southern Peruvian Altiplano. Geology, 33(7), 601–604.

Chen, T., and Clayton, R. W., 2009, Seismic attenuation structure in central Mexico: Image of a focused high-attenuation zone in the mantle wedge. Journal of Geophysical Research: Solid Earth, 114(B7).

Chlieh, M., Perfettini, H., Tavera, H., Avouac, J. P., Remy, D., Nocquet, J. M., ... & Bonvalot, S. (2011). Interseismic coupling and seismic potential along the Central Andes subduction zone. Journal of Geophysical Research: Solid Earth, 116(B12).

Delacour, A., Gerbe, M. C., Thouret, J. C., Wörner, G., & Paquereau–Lebti, P. (2007). Magma evolution of Quaternary minor volcanic centres in southern Peru, Central Andes. Bulletin of Volcanology, 69(6), 581–608.

Dobson, D. P., Meredith, P. G., & Boon, S. A. (2002). Simulation of subduction zone seismicity by dehydration of serpentine. Science, 298(5597), 1407–1410.

Dougherty, S. L., & Clayton, R. W. (2014). Seismic structure in southern Peru: evidence for a smooth contortion between flat and normal subduction of the Nazca Plate. Geophysical Journal International, 200(1), 534–555.

Eberhart-Phillips, D., and Chadwick, M., 2002, Three-dimensional attenuation model of the shallow Hikurangi subduction zone in the Raukumara Peninsula, New Zealand. Journal of Geophysical Research: Solid Earth, 107(B2).

Elger, K., Oncken, O., & Glodny, J. (2005). Plateau-style accumulation of deformation: Southern Altiplano. Tectonics, 24(4).

Faul, U. H., J. D. Fitz Gerald, and I. Jackson (2004), Shear wave

attenuation and dispersion in melt-bearing olivine polycrystals: 2. Microstructural interpretation and seismological implications, J. Geophys. Res., 109, B06202, doi:10.1029/2003JB002407

Gutscher, M. A., Spakman, W., Bijwaard, H., & Engdahl, E. R. ,2000, Geodynamics of flat subduction: seismicity and tomographic constraints from the Andean margin. Tectonics, 19(5), 814-833.

Kanamori, H., and Anderson, D. L., 1975, Theoretical basis of some empirical relations in seismology. Bulletin of the Seismological Society of America, 65(5), 1073-1095.

Haberland, C., & Rietbrock, A. (2001). Attenuation tomography in the western central Andes: A detailed insight into the structure of a magmatic arc. Journal of Geophysical Research: Solid Earth, 106(B6), 11151-11167.

Hansen, P. C., 1999, The L-curve and its use in the numerical treatment of inverse problems. IMM, Department of Mathematical Modelling, Technical University of Denmark.

Hayes, G. P., Wald, D. J., & Johnson, R. L. (2012). Slab1. 0: A three-dimensional model of global subduction zone geometries. Journal of Geophysical Research: Solid Earth, 117(B1).

Heit, B., Sodoudi, F., Yuan, X., Bianchi, M., & Kind, R. (2007). An S receiver function analysis of the lithospheric structure in South America. Geophysical Research Letters, 34(14).

Heit, B., Koulakov, I., Asch, G., Yuan, X., Kind, R., Alcocer-Rodriguez, I., ... & Wilke, H. (2008). More constraints to determine the seismic structure beneath the Central Andes at 21 S using teleseismic tomography analysis. Journal of South American Earth Sciences, 25(1), 22-36.

Kay, S. M., & Coira, B. L. (2009). Shallowing and steepening subduction zones, continental lithospheric loss, magmatism, and

crustal flow under the Central Andean Altiplano–Puna Plateau. Geological Society of America Memoirs, 204, 229–259.

Kim, Y., and Clayton, R. W., 2015, Seismic properties of the Nazca oceanic crust in southern Peruvian subduction system. Earth and Planetary Science Letters, 429, 110–121.

Lahr, J.C., 1999, revised 2012, HYPOELLIPSE: a computer program for determining local earthquake hypocentral parameters, magnitude, and first–motion pattern: U.S. Geological Survey Open–File Report 99–23, version 1.1, 119 p. and software, available at https://pubs.usgs.gov/of/1999/ofr–99–0023/.

Laske, G., Masters, G., Ma, Z., & Pasyanos, M. (2013, April). Update on CRUST1. 0—A 1-degree global model of Earth's crust. In Geophys. Res. Abstracts (Vol. 15, p. 20132658abstrEGU).

Lim, H., Y. Kim, and R. W. Clayton, .2015, December, Seismicity and structure of Nazca Plate subduction zone in southern Peru. In AGU Fall Meeting Abstracts.

Liu, M., Yang, Y., Stein, S., Zhu, Y., & Engeln, J. (2000). Crustal shortening in the Andes: Why do GPS rates differ from geological rates?. Geophysical Research Letters, 27(18), 3005–3008.

Ma, Y., & Clayton, R. W. (2014). The crust and uppermost mantle structure of Southern Peru from ambient noise and earthquake surface wave analysis. Earth and Planetary Science Letters, 395, 61–70.

Mamani, M., Wörner, G., & Sempere, T. (2010). Geochemical variations in igneous rocks of the Central Andean orocline (13 S to 18 S): Tracing crustal thickening and magma generation through time and space. Geological Society of America Bulletin, 122(1–2), 162–182.

Martinod, J., Guillaume, B., Espurt, N., Faccenna, C., Funiciello, F.,

& Regard, V, 2013, Effect of aseismic ridge subduction on slab geometry and overriding plate deformation: Insights from analogue modeling. *Tectonophysics*, *588*, 39–55.

McNamara, D. E., 2000, Frequency dependent Lg attenuation in south–central Alaska. Geophys. Res. Lett, 27(23), 3949–3952.

Menke, W., 2012, William. Geophysical data analysis: discrete inverse theory. Academic press

Mu¨ller, R. D., M. Sdrolias, C. Gaina, and W. R. Roest ,2008, Age, spreading rates, and spreading asymmetry of the world's ocean crust, Geochem. Geophys. Geosyst., 9, Q04006, doi:10.1029/2007GC001743.

Myers, S. C., Beck, S., Zandt, G., & Wallace, T. (1998). Lithospheric-scale structure across the Bolivian Andes from tomographic images of velocity and attenuation for P and S waves. Journal of Geophysical Research: Solid Earth, 103(B9), 21233–21252.

Phillips, K., R. W. Clayton, P. Davis, H. Tavera, R. Guy, S. Skinner, ... and V. Aguilar, 2012, Structure of the subduction system in southern Peru from seismic array data. Journal of Geophysical Research: Solid Earth, 117(B11).

Phillips, K., and Clayton, R. W., 2014, Structure of the subduction transition region from seismic array data in southern Peru. Geophysical Journal International, 196(3), 1889–1905.

Pozgay, S. H., Wiens, D. A., Conder, J. A., Shiobara, H., & Sugioka, H. (2009). Seismic attenuation tomography of the Mariana subduction system: Implications for thermal structure, volatile distribution, and slow spreading dynamics. Geochemistry, Geophysics, Geosystems, 10(4).

Prieto, G., R. Parker, F. Vernon, 2009, A fortran 90 library for

multitaper spectrum analysis, Computer&Geosciences, 35, 1701-1710

Ramos, V. A., Zapata, T., Cristallini, E., & Introcaso, A. (2004). The Andean Thrust SystemLatitudinal Variations in Structural Styles and Orogenic Shortening.

Ryan, J., Beck, S., Zandt, G., Wagner, L., Minaya, E., & Tavera, H. (2016). Central Andean crustal structure from receiver function analysis. Tectonophysics, 682, 120-133.

Rychert, C. A., Fischer, K. M., Abers, G. A., Plank, T., Syracuse, E., Protti, J. M., ... & Strauch, W. (2008). Strong along-arc variations in attenuation in the mantle wedge beneath Costa Rica and Nicaragua. Geochemistry, Geophysics, Geosystems, 9(10).

Scire, A., Zandt, G., Beck, S., Long, M., Wagner, L., Minaya, E., & Tavera, H. (2015). Imaging the transition from flat to normal subduction: Variations in the structure of the Nazca slab and upper mantle under southern Peru and northwestern Bolivia. Geophysical Journal International, 204(1), 457-479.

Schurr, B., Asch, G., Rietbrock, A., Trumbull, R., & Haberland, C. H. (2003). Complex patterns of fluid and melt transport in the central Andean subduction zone revealed by attenuation tomography. Earth and Planetary Science Letters, 215(1), 105-119.

Schurr, B., Rietbrock, A., Asch, G., Kind, R., & Oncken, O. (2006). Evidence for lithospheric detachment in the central Andes from local earthquake tomography. Tectonophysics, 415(1), 203-223.

Shito, A., & Shibutan, T. (2003). Anelastic structure of the upper mantle beneath the northern Philippine Sea. Physics of the Earth and Planetary Interiors, 140(4), 319-329.

Stachnik, J. C., Abers, G. A., & Christensen, D. H. (2004). Seismic attenuation and mantle wedge temperatures in the Alaska

subduction zone. Journal of Geophysical Research: Solid Earth, 109(B10).

Stein, S., and M. Wysession, 2009, An introduction to seismology, earthquakes, and earth structure. John Wiley & Sons.

Tarantola, A., 2005, Inverse problem theory and methods for model parameter estimation. Society for Industrial and Applied Mathematics.

Ward, K. M., Zandt, G., Beck, S. L., Wagner, L. S., & Tavera, H. (2016). Lithospheric structure beneath the northern Central Andean Plateau from the joint inversion of ambient noise and earthquake-generated surface waves. Journal of Geophysical Research: Solid Earth, 121(11), 8217-8238.

Whitman, D., Isacks, B. L., & Kay, S. M. (1996). Lithospheric structure and along-strike segmentation of the Central Andean Plateau: seismic Q, magmatism, flexure, topography and tectonics. Tectonophysics, 259(1-3), 29-40.

Abstract

페루 남부 나즈카 판 섭입대의 지진파 감쇠 구조

장효인
지구환경과학부
The Graduate School
Seoul National University

페루 남부의 나즈카 판 섭입대는 섭입 각도가 얕은 각도부터 급한 각도까지 바뀐다. 이러한 변화는 나즈카 능선의 섭입으로 인한 것이라는 추측이 있어 왔다. 우리는 PeruSE, PULSE, 그리고 CAUGHT의 세 개의 지진관측망을 사용하여 이 지역의 지진자료를 얻었다. 각각의 지진자료를 이용하여 P와 S파 각각의 지진파 감쇠값인 Q를 측정하였다. 우리는 우선 각 지진파에서 Q의 축적된 값의 합인 t*를 측정한 후 역산하여 삼차원 지진파 감쇠 구조를 구하였다.

역산된 지진파 구조는 페루 남부의 섭입구조, 형태 그리고 지질학적 특성과 밀접한 관련을 보인다. 첫째로, 대륙지각에서 상대적으로 큰 감쇠를 보여주었다. 특히 화산대와 동부 Cordilera 하부에서 마그마의 존재와 관련되어 보이는 아주 높은 감쇠를 보여주었다. 둘째로 섭입한 판의 탈수작용으로 보이는 낮은 감쇠값들이 화산대 하부에서 나타났다. 또한 지각과 섭입판 사이의 맨틀에서 떨어져 나온 지각으로 추정되는 높은 감쇠값을 가진 구조들이 발견되었다. 셋째로 나즈카 능선이 섭입하는 곳에서 탈수작용으로 보이는 낮은 감쇠값을 가진 구조가 관찰되었다.

Keywords : 지진파 감쇠 구조, 페루 남부, 나즈카 판 섭입
Student Number : 2016-20428